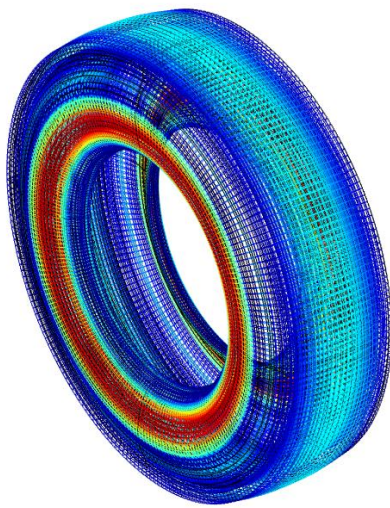


CHALMERS



Modelling the Vibration Behaviour of Truck Tyre

Master's Thesis in the Master's programme in Sound and Vibration

AMR ABOUD

Department of Civil and Environmental Engineering

Division of Applied Acoustics

Vibroacoustics research Group

CHALMERS UNIVERSITY OF TECHNOLOGY

Göteborg, Sweden 2014

Master's Thesis 2014:19

MASTER'S THESIS 2014

Modeling the vibration behavior of a truck tire

Amr Abboud

Department of Civil and Environmental Engineering
Division of Applied Acoustics
Vibroacoustics Group
CHALMERS UNIVERSITY OF TECHNOLOGY
Göteborg, Sweden 2014

Modeling the vibration behavior of a truck tire

© Amr Abboud, 2014

Master's Thesis 2014

Department of Civil and Environmental Engineering
Division of Applied Acoustics
Roomacoustics Group or Vibroacoustics Group
Chalmers University of Technology
SE-41296 Göteborg
Sweden

Tel. +46-(0)31 772 1000

Reproservice / Department of Civil and Environmental Engineering
Göteborg, Sweden 2014

Modeling the vibration behavior a of a truck tire

Amr Abboud

Department of Civil and Environmental Engineering

Division of Applied Acoustics, Vibroacoustics Group

Chalmers University of Technology

Abstract

Traffic noise is one of the major environmental issues that can affect a human's health, their comfort and productivity. One of the main sources of traffic noise is tire/road interaction noise, which become the most dominant sources if vehicle speed exceeds a certain level, e.g. 30 km/h for light vehicle and 50 km/h for heavy vehicle[18].

During the past decades, many studies were done on tires, trying to optimize these environmental issue, where several models and techniques for passenger car tires have been developed. However, less attention was paid to truck tires. The goal of this project was to build a numerical model that simulates the vibration behaviour of a truck tire in the modelling procedure of noise emission and rolling resistance. The model is based on the Finite Element approach taking most of the details of the tire structure into account, which can describe the complex vibration behaviour of truck tires. It modelled the vibration behaviour of tire structure in frequency range up to 500 Hz.

Solid mechanics methodologies, allow to calculate the mechanical parameters of tire components such as total bending stiffness. The tire model is a multi-physics Finite Element approach based on the solid mechanics module combined with the curvilinear mathematical approach. Based on the modal summation method the resulting data was processed to accomplish the mobility response function.

Driving point mobility and transfer mobility, which can be used to validate the simulation, get more information about tire properties, and deeper understanding of tire behavior, were also measured.

From these results it can be concluded that the measurement results, can successfully be used for further simulations of the contact force and noise radiation. While initial simulation results shows some deviation to measurements, important physical effect such as the influence of inflation pressure can successfully be modelled.

Keywords: finite element analysis, vibration response, point mobility, transfer mobility.

Contents

1	Introduction	1
2	Truck Tire Construction	2
3	Finite Element Modeling	4
3.1	Solving the FE discrete equation for solid mechanics	4
3.2	The WFEM- An overview	6
4	Solid Mechanics	7
4.1	Strain deformation relation for linear elastic material	7
4.2	Stress strain relationship, generalized Hooks law (Anisotropic Form)	8
4.2.1	Isotropic materials	8
4.2.2	Composite materials (Belts layers and Ply)	9
4.2.3	Curvilinear Coordinate	11
4.2.4	Damping model	12
5	Modeling producers	13
5.1	Geometry defeating	13
5.2	Meshing process	14
5.3	Inflation simulation	18
5.4	Free response simulation	18
5.5	Data post processing	19
6	Measuring the dynamic behavior of truck tire	20
6.1	Radial point mobility and transfer mobility measurements . . .	20
7	Results and discussion	23
7.1	Measurement results	24
7.2	Modeling results	28
7.2.1	Pressurization simulation	28
7.2.2	Eigenfrequency simulation	29
7.3	Simulated results and validation	30
8	Conclusions	35
9	References	36

Acknowledgement

I would like to thank my supervisor, Carsten Hoever, who has supported me throughout my thesis, with his valuable advice, guidance and understanding. He was always accessible, and willing to provide me with knowledge.

I would like provide all my appreciation to my brilliant teacher Wolfgang Kropp, for his continuous supporting and understanding, during the two wonderful years I have spent it in the acoustics division of Chalmers.

Thankfulness to Brje Wijk, for his help and support with lab equipment and for letting me borrow his tools and the computer

My grateful thanks are also extended to my wonderful colleges, I wish you all the best.

Words fail me to express my appreciation to my family, specially my parents, for believing in me, being unconditionally supportive, and whose foresight and values paved my way for a privileged education.

Finally, I would like to dedicate this thesis to my wounded country Syria, to the children and martyrs, and to the steadfast people who are making history nowadays, for justice and freedom.

1 Introduction

Background

Environmental impact of an automobile vehicle has been investigated as one of the major sources for urban noise pollution and greenhouse gas emission. Traffic noise pollution has become a growing concern to residents worldwide. This is particularly true in urban areas where the population density near major thoroughfares, and there is a greater volume of commuter traffic. Consequently, a substantial amount of research has been done. The noise produced from tire-pavement interaction is just one of several types of traffic noise. However, for roads with heavy vehicles travelling at speed of 50 km/h the noise due to tire-road interaction dominates [18].

Aim

The aim of this report is to investigate the possibility of building a numerical model that simulates the vibration behavior of a truck tire at low-mid frequencies, which is one of the mechanisms of noise generation as radiating structure. Further perform measurements on the same tire and trying to evaluate the quality of the computed results which is taken from the measurements and, finally perform a parameter study of the material properties and geometry of the structure.

The simulation was performed on a three dimension geometric model of [315/80 R22.5] Truck Tire, in this case all the parts of truck tire influence on the vibration mechanism.

Limitation

The general limitations of any numerical analysis, is the high calculation cost, and the requirement for high performance computing machines. It becomes more complicated for large complex geometries such as truck tire.

Material properties of tires in general it's hard to be recognized, since the rubber compounds changed completely after the vulcanization process make that challenging to extract mechanical properties such as Young's modulus.

During the past decades, many studies were done on car tires, however, fewer concentrate about truck tires make a validation of this study hard.

2 Truck Tire Construction

A tire is a composite of complex elastomer formulations, fibres, and steel cords.

Although rubber is the main material used for making tires there are a number of other components used as well. These materials are combined with rubber compounds in the different components that make up the tire's construction [21].

Tire construction and tire design are two key tire factors, which influence its vibration behaviour, noise, rolling resistance, wear and lifetime etc. A truck tire is a multilayer structure. A typical cross section is shown in figure 1. The outer components made up of rubber compounds, which has to provide the appropriate properties for the proper contact of the tire with a road. The inner component's layers are the skeleton of the tire, consist of several belts and plies, made up of steel fibres (cords) embedded in the rubber mixture[20][7]. Each component of a tire is designed to provide benefits specifically related to its function, while working together with all other components.



Figure 1: Truck tire cross section [20]

Belts and Ply layer

The model of the tire consists of four belts and one ply. The belts and ply are made up of steel fibers (cords) gives strength and stability to the tread area, which contributes to wear, handling and traction [21]. The belt system is placed on top of the casing in the construction process. While ply is the lowest fibre layer, extend all around the inner structure from bead to bead provides the side wall with appropriate strength. The steel cords in each layer and ply have a diameter of 0.15-0.4 mm and their number can vary in each belt[7] and are oriented with different directions [21].

Tread

The tread is a thick extruded section of rubber profile that surrounds the tire and make contact with the road surface. Tread is made of rubber with verity of additives compounds, and it has a certain patterns that give the tire traction to the road surface [21][7].

Sidewalls

The sidewalls are the parts of the tire that connect between the tread and beads. Made of a special rubber compound which is dissimilar from one used in the tread, this compounds adds more flexibility and weathering resistance[21]. The sidewall of the modelled tire, reinforced with steel cords of the ply, that provide for tensile strength and flexibility.

Bead

The bead is that part of the tire, that fit against the vehicle's wheel rim. They are large steel cords that are twisted together to form a cable in a ribbon-type configuration.

3 Finite Element Modeling

The finite element method (FEM) is a computer technique for solving partial differential equations numerically, uses variational methods to minimize an error function and produce a stable solution, and consequently predicts the deformation and stress fields within solid bodies subjected to external forces, as it defined by Alan F. Bower [15].

3.1 Solving the FE discrete equation for solid mechanics

The principle of Finite Element Method is to approximate the continuous system into a discrete system by subdividing into smaller, more manageable finite elements. The objective is to calculate the displacement field $u(x)$ specifies the motion of the point at position x in the undeformed solid [15]; thus, the objective is to determine $u(x)$. The process of dividing the structure into discrete elements is called 'discretization'. Interpolation within the elements is achieved through shape functions. Once $u(x)$ is known, the strain and stress fields in the solid can be deduced[15].

For static problems the finite element method, based on solving the equilibrium equations $\sum F = 0$. where for dynamic problems, the finite element method solves the equations of motion for a continuum, which is a more complicated version of ($\sum F = m \cdot a$).

The simulation of this project, was mainly carried out using Solid Mechanics module in Comsol Multiphysics V.4.3b. COMSOL Multiphysics bases its implementation of structural mechanics application modes, on the equilibrium equations expressed in global stress components.

The equilibrium equations expressed in the stresses for 3D Cartesian coordinate are :

$$\frac{-\partial \sigma_x}{\partial x} + \frac{-\partial \tau_{xy}}{\partial y} + \frac{-\partial \tau_{xz}}{\partial z} = F_x, \quad (1)$$

$$\frac{-\partial \tau_{xy}}{\partial x} + \frac{-\partial \sigma_y}{\partial y} + \frac{-\partial \tau_{yz}}{\partial z} = F_y, \quad (2)$$

$$\frac{-\partial \tau_{xz}}{\partial x} + \frac{-\partial \tau_{yz}}{\partial y} + \frac{-\partial \sigma_z}{\partial z} = F_z, \quad (3)$$

Where F is the volume force, $(\sigma_x, \sigma_y, \sigma_z)$ are normal stress components, and $(\tau_{xy}, \tau_{xz}, \tau_{yz})$, are shear stress components. By using the compact notation, the previous relations can be rewritten as

$$-\nabla \cdot \sigma = F \quad (4)$$

Where σ is the stress tensor. the stress-strain relationship and the strain-displacement relationship will be substituted into Navier's equations [17].

Analysis of free vibration

In free vibration analysis the eigenfrequency, f , and eigenmodes ϕ_i of free vibration of the structure is determined by solving the eigenvalue problem in eq(5). In the eignfrequency analysis, the mass is added to the modelled system. Eigenfrequency is obtained by solving the following equation for the eigenvalue λ [17]:

$$-\lambda d_a u - \nabla \cdot c \nabla u = 0, \quad (5)$$

the d_a in equation 5 is the density coefficient, and c is the static coefficient. The eignfrequency f is related to the eigenvalue λ by:

$$f = \frac{\sqrt{\lambda}}{2\pi} \quad (6)$$

frequency domain analysis

In the frequency domain, the frequency response is studied when the system is excited with harmonic loads F_{freq} . Harmonic loads are determined by the amplitude A , and phase (Φ).

$$F = A \cos(\omega.t + \Theta) \quad (7)$$

$$F = \begin{bmatrix} F_x \\ F_y \\ F_z \end{bmatrix}$$

the forced response is a harmonic response assumed to have the same angular frequency as the excitation load.

$$u = u_{amp} \cos(\omega.t + \Phi) \quad (8)$$

3.2 The WFEM- An overview

The wave guide finite element analysis, is a numerical method applied to solid structures or fluid systems was developed by Finnveden and Nilsson, and has been used a lot for modeling the vibration behavior of tires. As suggested by the name, an approach by which approximate wave solutions are found for objects acting as wave-guides. To be specific, this method uses the finite element model over a cross section to come at a set of coupled partial differential equations (PDE) to which source free solutions have the physical interpretations of waves Ref [3].

By setting $F = 0$, the homogeneous case is obtained to, which free response solutions to the wave guide FE-equation solved for the twin parameter eigenvalue problem in angular frequency ω and wave number k for which two solution strategies exist.

The main advantage of the WFEM as compared to FE formulation is that decrease the calculation burden. this argument comes from the fact that the only cross section is discretized, reducing the number of degree of freedom introduced to the model [3]. An additional advantage compared to conventional FE is that different wave-type are easy to identify and analyse, allowing for some easier interpretation and easier understanding for physical behaviour of tire structure.

This report doesn't show a complete comparison between conventional FEM and WFEM, however the advantage of the parameters ω and k from WFEM in describing of the physical behaviour of the tire will be used to describe the mode shape in the modelling results.

4 Solid Mechanics

Solid Mechanics is a collection of physical laws, mathematical techniques, and computer algorithms that can be used to predict the behaviour of a solid material that is subjected to mechanical or thermal loading [15], [12].

4.1 Strain deformation relation for linear elastic material

Describing a relative small displacement of a deformed point with the deformation components (u, v, w) in 3D and their derivatives is done in the form of symmetric strain tensor, which consist of the normal strain components $(\varepsilon_x, \varepsilon_y, \varepsilon_z)$ and the shear strain components $(\varepsilon_{xy}, \varepsilon_{xz}, \varepsilon_{yz})$. The symmetric strain tensor can be written in a matrix form as

$$\boldsymbol{\varepsilon} = \begin{pmatrix} \varepsilon_x & \varepsilon_{xy} & \varepsilon_{xz} \\ \varepsilon_{xy} & \varepsilon_y & \varepsilon_{yz} \\ \varepsilon_{xz} & \varepsilon_{yz} & \varepsilon_z \end{pmatrix} \quad (9)$$

The stress of a material is described by the symmetric stress tensor

$$\boldsymbol{\sigma} = \begin{pmatrix} \sigma_x & \tau_{xy} & \tau_{xz} \\ \tau_{xy} & \sigma_y & \tau_{yz} \\ \tau_{xz} & \tau_{yz} & \sigma_z \end{pmatrix} \quad (10)$$

consisting of three normal stresses $(\sigma_x, \sigma_y, \sigma_z)$, and six shear stress $(\tau_{xy}, \tau_{xz}, \tau_{yz}, \tau_{yx}, \tau_{zx}, \tau_{zy})$. Due to symmetric property, the shear stress and strain component can be reduced to three.

$$\boldsymbol{\varepsilon} = \begin{bmatrix} \varepsilon_x \\ \varepsilon_y \\ \varepsilon_z \\ \varepsilon_{xy} \\ \varepsilon_{xz} \\ \varepsilon_{yz} \end{bmatrix} \quad (11)$$

$$\boldsymbol{\sigma} = \begin{bmatrix} \sigma_x \\ \sigma_y \\ \sigma_z \\ \tau_{xy} \\ \tau_{xz} \\ \tau_{yz} \end{bmatrix}$$

(12)

$$(\tau_{xy} = \tau_{yx}, \tau_{yz} = \tau_{zy}, \tau_{xz} = \tau_{zx}).$$

4.2 Stress strain relationship, generalized Hooks law (Anisotropic Form)

Cauchy generalized Hooke's law to three dimensional elastic bodies and stated that the 6 components of stress are linearly related to the 6 components of strain.

The stress-strain relationship for linear conditions is written in a matrix form as:

$$\sigma = D \cdot \epsilon \quad (13)$$

σ : is the stress tensor, ϵ is total strain tensor D is a fourth order tensor, which due to symmetry it can be completely represented by a symmetric 6×6 matrix, thus 36 stiffness components for any linearly elastic medium.

$$D = \begin{bmatrix} D_{11} & D_{12} & D_{13} & D_{14} & D_{15} & D_{16} \\ D_{21} & D_{22} & D_{23} & D_{24} & D_{25} & D_{26} \\ D_{31} & D_{32} & D_{33} & D_{34} & D_{35} & D_{36} \\ D_{41} & D_{42} & D_{43} & D_{44} & D_{45} & D_{46} \\ D_{51} & D_{52} & D_{53} & D_{54} & D_{55} & D_{56} \\ D_{61} & D_{62} & D_{63} & D_{64} & D_{65} & D_{66} \end{bmatrix}$$

(14)

However, is a result of the existence of a strain energy density function which satisfies $\sigma = \frac{\partial w}{\epsilon}$ where (w) is energy. Hence, stiffness and compliance matrices are symmetric. Therefore, only 21 stiffness components are actually independent in Hooke's law

The determination of D_{ij} values is dependent on the material characteristics for the specific layer. Large part of the tire, including the rubber in the tread and side walls, can be considered as homogeneous and isotropic, while the belt layers, and the ply, which is a fibrous composite, i.e. consist of steel fibres (also called cords) embedded in a rubber matrix. is considered as heterogeneous and depending on the angle between the fibre and the global coordinate system, thus locally orthotropic material [15].

4.2.1 Isotropic materials

The definition of Isotropic martial sates that material properties are independent of direction. The homogeneous isotropic the stiffness matrix is reduced to

$$D_{ij} = \begin{bmatrix} D_{11} & D_{12} & D_{12} & 0 & 0 & 0 \\ D_{12} & D_{11} & D_{12} & 0 & 0 & 0 \\ D_{12} & D_{12} & D_{11} & 0 & 0 & 0 \\ 0 & 0 & 0 & D_{44} & 0 & 0 \\ 0 & 0 & 0 & 0 & D_{44} & 0 \\ 0 & 0 & 0 & 0 & 0 & D_{44} \end{bmatrix}$$

(15)

Where properties are independent of direction, two independent variables are required to construct the stiffness matrix [15]

4.2.2 Composite materials (Belts layers and Ply)

The belt's layer and ply are fibrous composite material, consist of continuous steel fibres embedded in a matrix (rubber), the determination of the mechanical properties are a multi-step procedure, a classical approximation of a unidirectional continuous fibre composite mechanical properties takes from the rule of mixture and Halpin-Tsai equations [18] [12]. By assuming equal strain in fibre and matrix phases. The constituting materials of the layers are assumed to be homogeneous and isotropic. The properties are calculated with respect to the local coordinate system (see figure 2), where the axis 1 is along the direction of the fibres, the axis 2 is in a plane normal to the cord direction, and axis 3 out of plan direction. Young's modulus in the cord direction, E_1 , and Poisson ratio ν_{12} are directly estimated using the rule of mixture as following

$$E_1 = E_f V_f + E_m V_m \quad (16)$$

$$\nu_{12} = \nu_c V_f + \nu_m V_m \quad (17)$$

Herein, E_f , ν_f and E_m , ν_m are Young's modulus, Poisson ratios of the steel fibres and the matrix, respectively , V_f steel volume fracture, and V_m matrix volume fracture, which determined by using the following:

$$V_f = \frac{\vartheta_f}{\vartheta_f + \vartheta_m} \quad (18)$$

$$V_m = 1 - V_f \quad (19)$$

Where ϑ_f and ϑ_m are the volume of the fibers and the matrix,respectively. Halpin-Tsai technique is used for determining the corresponding mechanical properties for the second and third directions as following :

$$\frac{P^-}{P_m} = \frac{(1 + \zeta \eta V_f)}{(1 - \eta V_f)} \quad (20)$$

$$\eta = \frac{\left(\frac{P_f}{P_m} - 1\right)}{\left(\frac{P_f}{P_m} + \zeta\right)} \quad (21)$$

In these formulas, the quantities P^- , P_f , P_m , and ζ .

- P^- : composite moduli, E_{22} , G_{12} , or G_{23} , (G shear modulus)
- P_f : corresponding Fiber modulus, E_f , G_f

- P_m : corresponding matrix modulus, E_m, G_m
- ζ : an engineering constant depends on the boundary conditions, which reflect fiber reinforcement parameter and modulus influence on the elastic coefficients.

Halpin-Tsai model specifies a set of equations for the engineering constants ζ and each equation in the set has a default value for ζ , described as followed

$$\zeta_{G_{12}} = 1 + 40.V_f^{10} \quad (22)$$

$$\zeta_{E_{22}} = 2 + 40.V_f^{10} \quad (23)$$

$$\zeta_{G_{23}} = \frac{1}{4 - 3\nu_m} \quad (24)$$

according to Halpin-Tsai theory, the oriented continuous fibre's model, ν_{23} can be approximated as:

$$\nu_{23} = 1 - \frac{E_2}{G_{23}} \quad (25)$$

finally ν_{21} is determined by reciprocity:

$$\nu_{21} = \frac{\nu_{12}E_2}{E_1} \quad (26)$$

from equations 16 to 26, we can construct the stiffness matrix, and set the stress strain relationship for an orthotropic fibre composite on local coordinate (1,2,3).

$$D_{ij} = \begin{bmatrix} D_{11} & D_{12} & D_{13} & 0 & 0 & 0 \\ D_{12} & D_{22} & D_{23} & 0 & 0 & 0 \\ D_{13} & D_{23} & D_{33} & 0 & 0 & 0 \\ 0 & 0 & 0 & D_{44} & 0 & 0 \\ 0 & 0 & 0 & 0 & D_{55} & 0 \\ 0 & 0 & 0 & 0 & 0 & D_{66} \end{bmatrix}$$

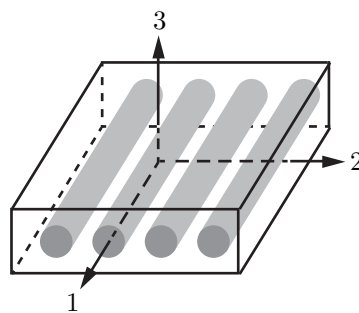


Figure 2: Fibrous composite layer with its local Cartesian coordinate system ([15] page 56).

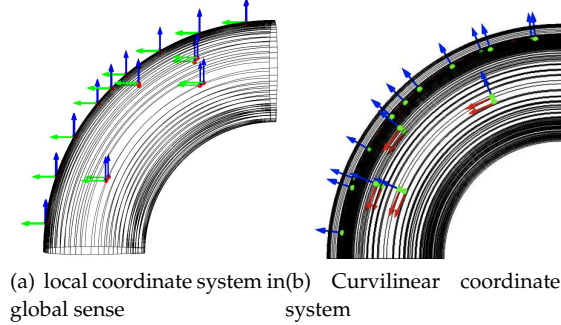


Figure 3: Comparison between the global coordinate system, and the curvilinear coordinate system.

4.2.3 Curvilinear Coordinate

Constructing a local coordinate system along the belt's cords is not straightforward procedure, particular matrices need to be defined for complicated structure like a tire belt. The cords in belts and ply are not only rotated along tire circumference, they are also angled with different direction around the normal axis in figure 2 in each layer. To solve this matter, Curvilinear coordinate system has been used to construct the local coordinate system in belts and ply.

Curvilinear Coordinates: is a system is a type of coordinate system, where the coordinate lines can be curved. The curvilinear basis vectors are defined from the tangent vectors, obtained by differentiating the Cartesian position with respect to the cylindrical coordinates.

$$\begin{aligned} e_r &= \frac{\partial x}{\partial r} = (\cos\phi, \sin\phi, 0) \\ e_\phi &= \frac{1}{r} \frac{\partial x}{\partial \phi} = (-\sin\phi, \cos\phi, 0) \\ e_z &= \frac{\partial x}{\partial z} = (0, 0, 1) \end{aligned} \quad (27)$$

As may be directly verified, they are orthogonal and normalized everywhere, and thus define a local curvilinear basis with an orientation that changes from place to place. COMSOL Multiphysics curvilinear user interface used to create the vector field v and a base vector system (e_r, e_ϕ , and e_z), that can be used by solid mechanics physics to specify the anisotropic material properties of a bundle of wires in belts and ply. The resulting coordinate system can be curvilinear fitting into the non-defined shape of those elements. figure 3 shows a comparison between the global coordinate system on the tire element and the curvilinear coordinate system on tire elements

4.2.4 Damping model

Damping is a dissipation of a mechanical energy of a dynamic system. Different model of damping describes the damping mechanism in the system.

The damping in the tire structure is mainly due to the rubber, which is modelled as an internal structure damping, two models of internal structure damping has been used for different studies.

Structure/hysteretic damping is associated with internal friction of the internal plans as the body deformed, it is proportional to the amplitude of displacement of the deformed body. It's independent of the frequency of the vibration[5],[9]. The Stress-Strain curve is plotted as shown in figure(4), the energy loss ΔU per cycle of motion is the area within the loop.

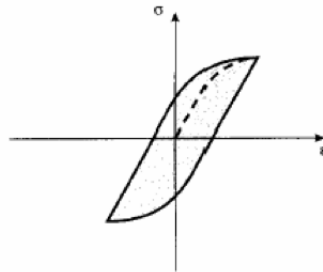


Figure 4: Hysteretic loop in stress strain.

Viscous/Raylieh damping: the Rayleigh damping model defines the damping parameter c in terms of the mass m and the stiffness k as

$$C = \alpha M + \beta K \quad (28)$$

Where α and β are real scalars with 1/sec and sec units respectively. Given the system mass, stiffness and damping matrices, the response of the system can be calculated. However, the accuracy of response may be questionable due to the fact that this approach is based on two main assumptions, a) The model used for damping of a structure is viscous and b) the approach is formulated for the linear response of the structure which may not be the available situation for all cases (i.e. structures with nonlinearities)[19]

Since it is not possible to completely present the consequences of damping model in structures in this report, the effects of usage of damping model in structures will not be considered.

5 Modeling producers

The vibration analysis of the truck tire is a multi-step procedure. First, it started with pressurizing the internal boundary of the tire, by performing a stationary load simulation, afterwards the eigenfrequency and frequency domain analysis will be executed. Linear elastic material laws, were applied for both rubber layers, and belt's layers (composite layers).

5.1 Geometry defeaturing

Due to the geometrical complexity of the tire cross-section, the meshing process can't be performed directly; therefore, the cross section of the tire has to be divided into several sections. This process helps to achieve a better mesh quality, and less number of nodes; consequently less calculations cost and more stability in calculation process. The modified cross-section is shown in figure 5 . Tread is divided into a three rectangular section, shoulders and sidewalls are also divided into several rectangular sections. All these modifications were done in order to get more flexibility in the meshing process and helps to achieve better mesh quality. On the other hand, the ply is divided into many small rectangles (See figure 5), that has done in order to achieve the desired local coordinate system, where several problems were faced during the solving process when using the curvilinear coordinate system

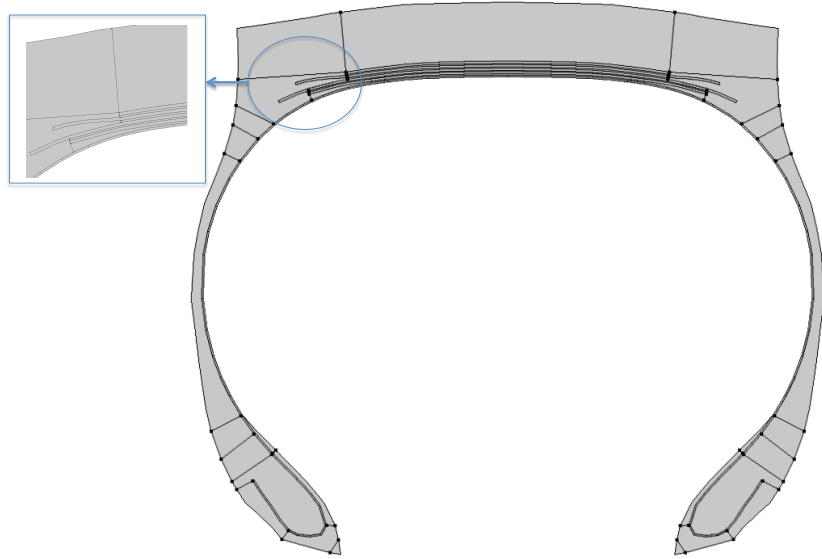


Figure 5: Defeaturing the cross section of the tire .

5.2 Meshing process

Meshing the tire structure, first was done by generating a 2D mesh on the tire cross-section in figure 5. This includes tread belts and sidewalls, air cavity and rim were excluded from the vibration analysis. However, the air pressure has been modelled as load per unit area acting on the internal boundary of the tire structure, where the rim displayed as a fixed support boundary blocking the motion of tire beads in 3D directions. The 2D meshing structure (figure 11) was assigned as a source face for the sweeping process to generate solid mesh for the 3D structure (figure ??).

Element formulation

The elements configurations in the tread sections, belts and, sidewalls have a structured shape and, doesn't include any discontinuities (that is no holes). Mapping technique was used, which create structured quadrilateral mesh on boundaries. The undefined shape sections, i.e. Shoulders and Beads, was meshed with unstructured quadrilateral and triangular elements. See figure 11 .

Discretization, Shape Function and Element Orders

The PDE and weak form interfaces have different shape functions available in Comsol, with the associated element order. A set of polynomial functions is used to approximate the structural displacements fields which describe how much the object deforms in each of the three coordinate directions. The complexity of the model and the limited time and cost resources, narrows the number maximum used elements, which led to a number of elements with high aspect ration (elongated elements), that encourages COMSOL to create a number of inverted elements, which make it better to use shape elements. On the other hand, the accuracy of the solution is linked to the mesh quality. With an appropriate mesh, the solution will converge toward the approximated accepted solution, which is defined by certain error tolerance. However, because of those mentioned limitations the resultant mesh quality can't guarantee a good or accurate solution.

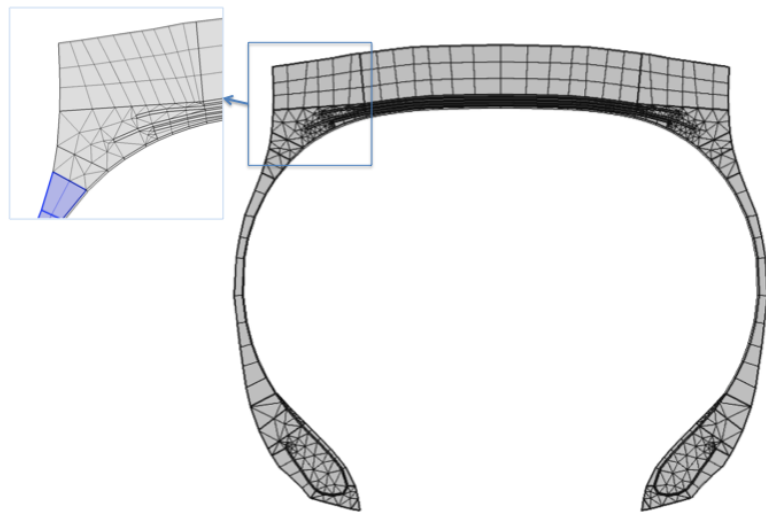


Figure 6: Meshing the cross section of the tire .

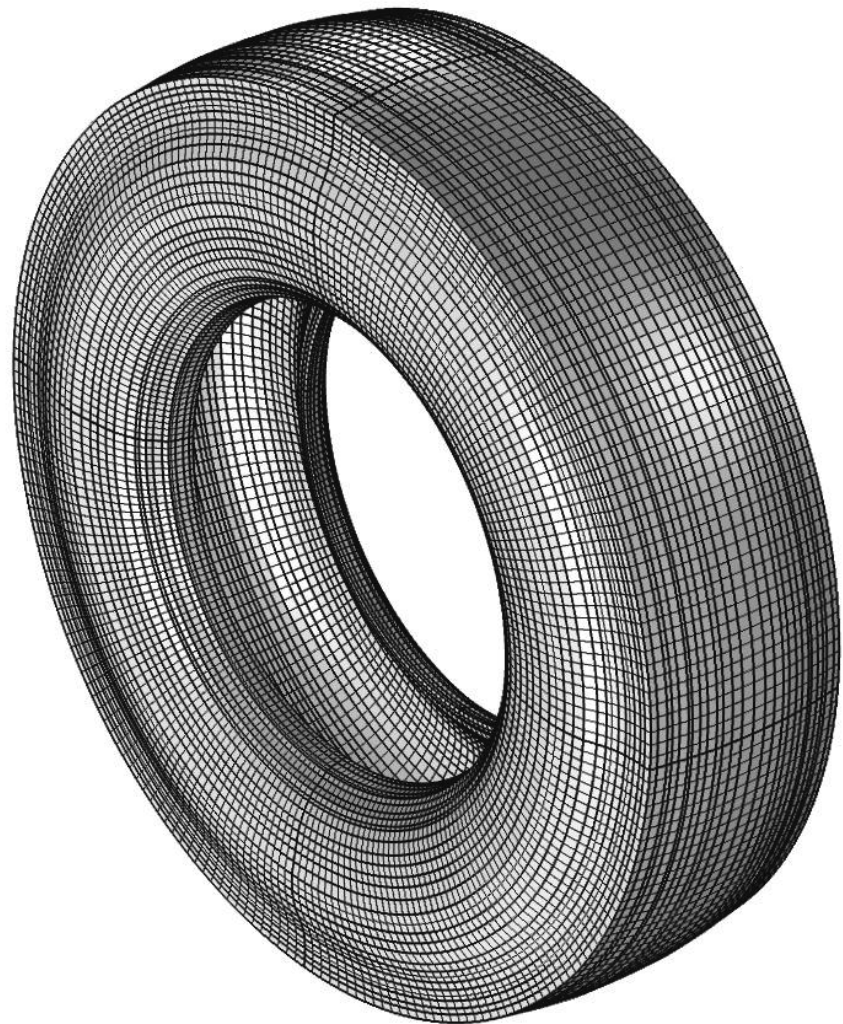


Figure 7: The complete meshed model of the tire.

Lagrangian formulation

The formulation used for structural analysis in COMSOL Multiphysics for both small and finite deformations is total Lagrangian [17]. This means that the computed stress and deformation state, is always referred to the material configuration, rather than to the current position in space. Likewise, material properties are always given for material particles and with tensor components referring to a coordinate system based on the material frame. This has the obvious advantage that spatially varying material properties can be evaluated just once for the initial material configuration, and do not change as the solid deforms and rotates [17].

5.3 Inflation simulation

The stress distribution, which caused by the intake pressure, influences the calculation results of the dynamic behavior of the tire. Simulating the inflation process was done by performing a boundary load per unit area (P [Pa]), on the internal boundaries of the tire model, that resemble the air pressure of the inflated tire.

Parametric continuation solver is used to find the solution to a sequence of pressure parameters (in a range of 100 parameters), this way, the nonlinear solver gets a good initial guess based on the solution from the previous parametric values, and converge to the right solution. Few of these parameters were extracted for the vibration simulation, which are equivalent to the pressure values of the tire in experimental work.

Direct fully coupled solver used with stationary solver. Direct linear system solver is a matrix resolution algorithm, which computes the solution in a single step. The methodology was always based on the Gaussian elimination method, or LU factorization. Comsol has different direct solvers and iterative solver, since a non linear is going to be processed, direct solvers will be chosen. However, many direct solvers are available in Comsol and choosing the right solver is important for nonlinear complex calculation, in order to achieve the right solution efficiently, and avoid memory failure during the calculation process. The package PARDISO is used for it's a high-performance, robust, memory-efficient and easy to use software for solving large sparse symmetric and nonsymmetric linear systems of equations on shared memory and distributed-memory [17]. Fully coupled solver operates on the full Jacobian matrix as one entity, is generally requires less iterations but takes up more memory and solution time per iteration. The Fully Coupled uses a damped version of Newtons method, where solver automatically determine a damping factor in each iteration of Newtons method [16].

5.4 Free response simulation

Eigenfrequency study was the second step in the analysis. It solves the eigenvalue problem eq.5, for a set of eigenmodes and associated eigenfrequencies. The results from inflation study step, used as an initial parameter combined the eigenfrequency solver configuration, then compiling the equations to be solved, that allows to extract 10 eigenmodes corresponds to maximum eigenfrequency of 230 Hz , to be substituted in the second step .

5.5 Data post processing

Resultant data from the free response analysis, used for post processing step in order to extract the mobility function. The procedure started by extracting the displacement u using modal summation analysis taking advantage orthogonality property of mode shapes as follow

$$u = \sum_{n=1}^N \frac{\phi_n^T(\text{receiver}).\phi_n(\text{excitation})F}{\omega_n^2 - \omega^2 + i\eta\omega_n^2} \quad (29)$$

where F is the radial excitation force, η is the damping loss factor which is assigned to a constant value of 0.5, and ϕ : is the mass normalized mode shape of the mode ψ . $\phi = m_r^{0.5}\psi$. m_r is modal mass, which is given by orthogonality relation

$$\delta = \psi_m^H m_r \psi_n \quad (30)$$

Where δ is the Kronecker symbol.

Equation (29) permits to calculate the responses under point excitation. The resulting vector of responses is sometimes refereed as force vibration mode or operation deflection shape (ODS).

Taking time derivative of X and divided by force yields mobility, which can be either point or transfer mobility, depend on the choice of ϕ^T , which in role can either at the excitation point or response point.

6 Measuring the dynamic behavior of truck tire

Measuring the dynamic behavior of the truck tire is not only important for the validation process, it gives more information about the real tire behavior, as well deep understanding of the processes involved. To obtain these information, measurements of radial mobility, tangential mobility, including both driving point mobility and transfer mobility were made.

The measurements were carried out on a commercial truck tire type, 315/80 R 22.6, See figure (8) and figure (9). The experiments were performed in the vibroacoustic lab, the division of applied acoustics at Chalmers Institute of Technology, Gothenburg, Sweden.



Figure 8: 2. Measurement setup



Figure 9: 2. Measurement setup

6.1 Radial point mobility and transfer mobility measurements

Measuring the dynamic behavior of the tire is a typical measurement of dynamic behavior of any structures. special equipment were used during the measurements, are listed below

Equipment list

- Force Transducer: *B&K*type 8203
- Four pre-amplified accelerometers: *B&K* type 4517
- Conditioning Charge Amplifier: *B&K* type 2635
- Shaker: LDS V102
- Acquisition station: VXI
- Super clue: Type Luctide 4709
- Aluminum plate: dimensions 16×16 mm

The tire was freely suspended by four steel cables on a metal rack, as can be seen on figure 9 . The tire structure was excited by a force transducer through an Aluminum plate clued tire tread surface , with an external force $F(t)$. The force transducer produces a steady state response consisting of a superposition

of all the modes of vibrations and their corresponding natural frequencies. Fixing the Aluminum plate, was done by using superglue type Luctite 4709. The gluing method and size of the plate play an important role in the measurements results quality. The curvature of the tire as well the air gap between the tire tread and the plate shows an influence on the measured response.



Figure 10: The measured positions of transfer mobility in lateral direction

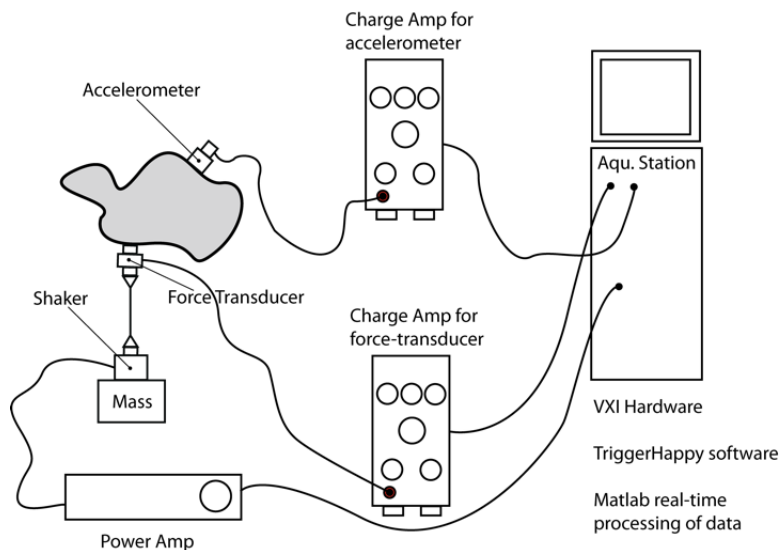


Figure 11: Sketch illustrate the laboratory equipment .

Transfer mobility was measured at different circumferential positions at (30, 45, 90, 120, and 180) degree, in each circumferential position, mobility was measured at six different lateral positions, as depicted in figure ?? . The measurements were investigated under different internal pressure started [1 bar, 2 bar, 3 bar, 4 bar, 5 bar, 6.7 bar] .

One accelerometer captured the transfer mobility signal, this accelerometer was fixed on the tread surface using accelerometer wax type 'Endevco Wax 32279', it is flexible and easy to use, but doesn't provide with the same gluing strength as superglue, which possibly can affect the quality of the measurement results.

The data is acquired by acquisition station, and analyzed through a software tool called TriggerHappy, which runs through a real-time processing Matlab program. Two different sets of measurements correspond to two different block size N_s : 32768 and 16000, which related to a frequency range (FR) 2000 Hz and 5000 Hz respectively. The results were extracted after averaging 20 samples for each measurement set. Damping was calculated using half-power band width method, in order to obtain some values, that will be used in the simulation later on.

7 Results and discussion

In this section the result from lab experiment, simulation of the finite element model and the validation of the modelling results will be presented. Section 7.1 present the results of experiments , while Section 7.2 will show the modelling results including the static simulation and the dynamic simulation. Finally, the validation of the simulation, and comparisons with measurements will be shown in section 7.3

7.1 Measurement results

The mobility was investigated at different pressure levels. See figure 12, which shows point mobility plots at different pressure levels. From figure 12, it can be noted that, the eigenfrequency become higher as pressure increases, which indicate that the stiffness of the structure increases by increasing the stress on it. This effect can be clearly seen, by investigating the first eigenfrequency, for each load case. However, the graphic results also shows, that the pressure effect on the point mobility becomes unremarkable in frequency range above 400 [Hz].

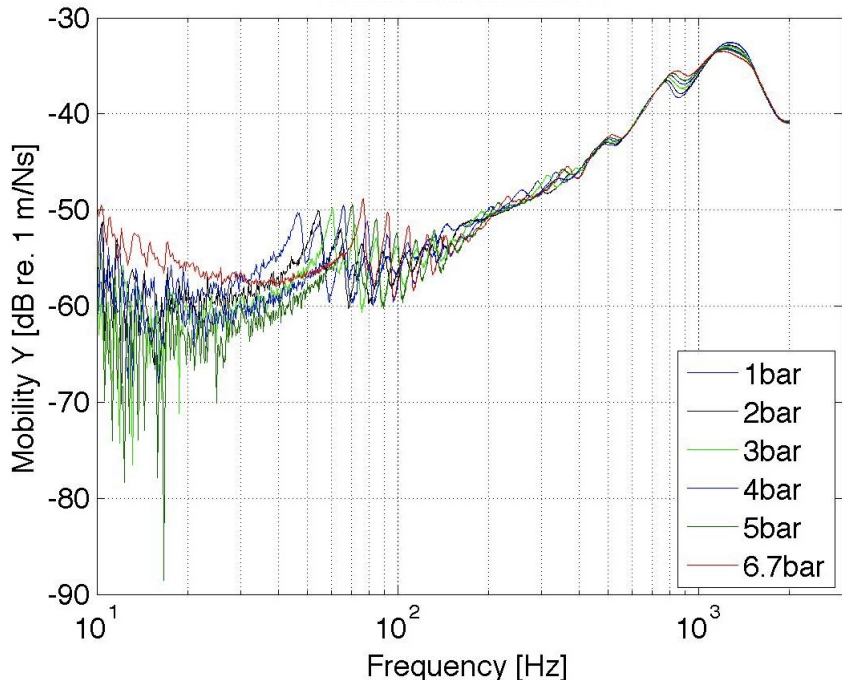


Figure 12: Measured point mobility at different pressure levels .

At frequencies higher than 300 Hz the point mobility response increases 6 dB per octave, which is related to the stiffness from the tread. In this frequency region the mass of the equipment together with tread stiffness forms a spring mass system. The tread stiffness initiation effect in the frequency response function, is connected to the size of the excitation plate, and that explains the reason of the increasing in magnitude above 200 Hz[2] .

The results of measured transfer mobility under the same pressure levels can be seen in 13 . The results show that transfer mobility is affected by the same manner as point mobility under the different pressure levels, still it can be seen the pressure effect becomes unremarkable in frequency range above 400 [Hz].

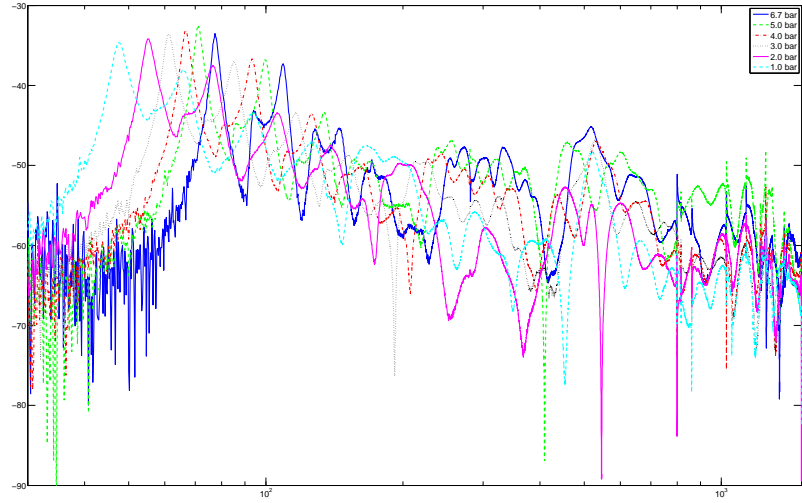


Figure 13: Measured transfer mobility at different pressure levels .

Figure 14 shows comparison between drive point mobility and transfer mobility for the different circumferential positions which have mentioned previously. In frequency range from 10 Hz up to 2000 Hz, the difference in response can be explained by modal vibration behavior of the tire. Measured point close to a nodal line of a particular mode, has a lower magnitude than one measured at a point close to an anti-nodal line. In this frequency range, the tire modal behavior consists of different symmetric and ant-symmetric modes.

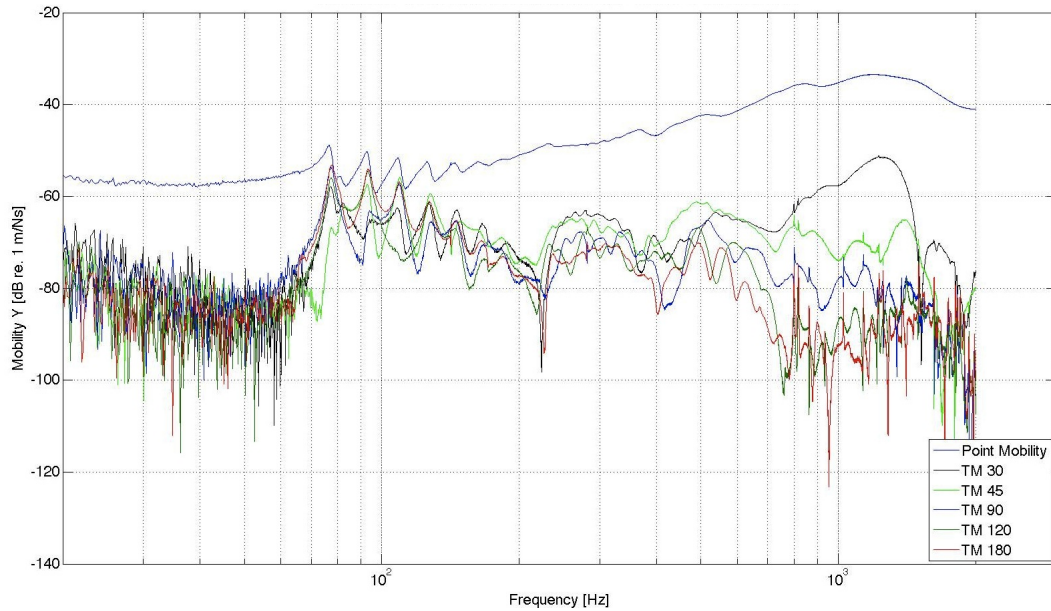


Figure 14: Comparison between point mobility and transfer mobility in the circumferential direction for different angels, from 30 to 180 degrees.

The evaluation result of transfer mobility of different lateral positions are presented in figure 15. Back from figure 10, the excitation point was located on the middle of tread on line 3 (Position 3), position 1 and position 2 as it referred in figure 10 as (Pos1) and (Pos2) refer to the uppermost response point, while position 5 and 6 (Pos 5 and Pos 6) are the lowest response point.

In mid range frequency, the magnitude of the mobility decrease with distance, this can be explained by a different type of damping mechanisms involve in this frequency range. However, the value position 6 is relatively has lower level compared to the other positions of transfer mobility, this due to the longer distance as well the poor fixation of the accelerometer on the smooth tread surface. Finally, the total vibration pattern, is a result of reflected and diffracted waves.

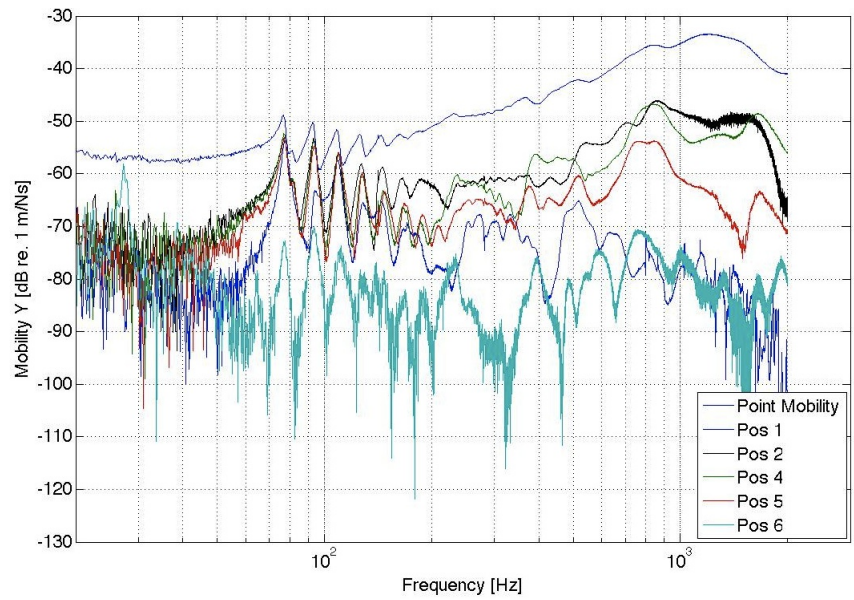


Figure 15: Magnitude of transfer mobility measured in lateral directions.

7.2 Modeling results

In this section results from Finite Element Model (FEM), and a comparison between the measured and modeled results will be presented. The static tire inflation simulation will be presented in section 7.2.1. Section 7.2.2 will present the results of free response simulation, and section 7.2.3 shows the forced frequency response modeling results, and comparison between modeled results and measured results.

7.2.1 Pressurization simulation

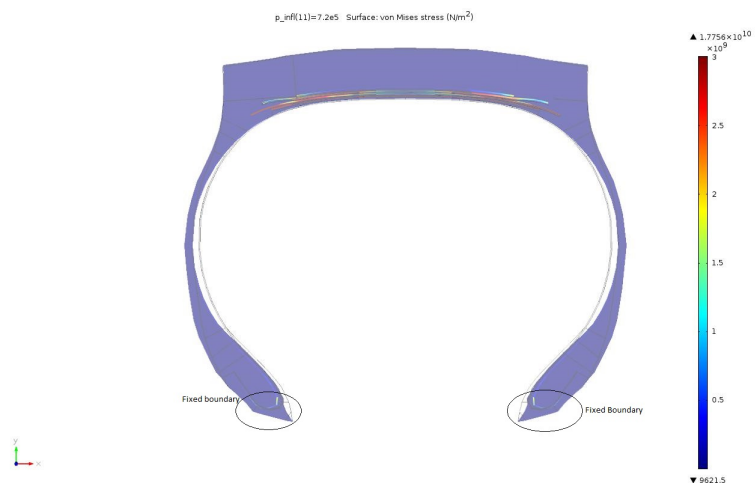


Figure 16: Diformation and stress distribution of tire structure under internal pressure of 7.2 bar.

Simulating the inflation process of the tire was performed, by applying parametric loads per unite area equivalent to the parameters in the experiment, on the internal boundary of the tire. The boundaries on the bead area were totally fixed . From this simulation, the equivalent stress and deformation are extracted. From figure ?? the results shows stress concentration on belt's region, and more deformation arises on sidewalls, maximum deformation was 4 [mm], in the mid region of a side wall. These results of each pressure step are going to be used as pre-tension step for eigenfrequency analysis.

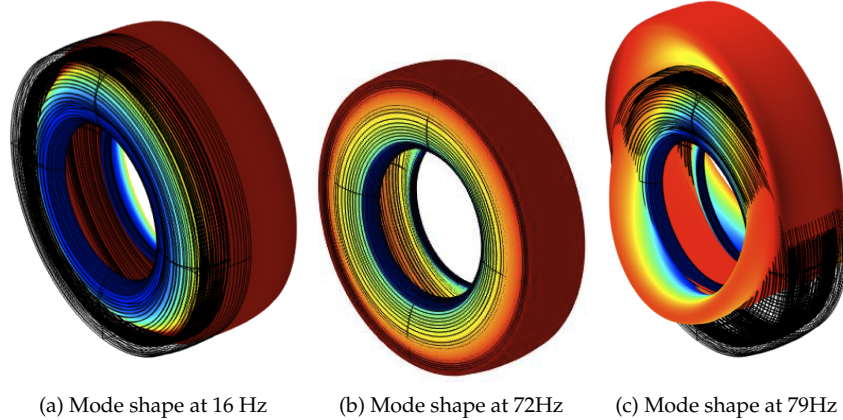


Figure 17: Semi rigid body motion modes

7.2.2 Eigenfrequency simulation

In the eigenfrequency analysis semi-rigid mode can be extracted beside the other modes. The first frequency range is low vibration frequencies, reflecting the first four lower eigenfrequencies. The corresponding mode shapes are semi-rigid body motion, the tread and belts act as a rigid ring and the side-walls act as supporting spring, some of these modes are shown in figure 17 and the rest of the 3D plots are displayed in figure 1 and 2 in appendix A. The first mode seen at $k=0$, corresponds to the displacement of the rigid ring along the axis of revolution (x-axis) Figure 17. The second mode having a value of $k=0$, this mode involves a rotation of the ring around the x-axis it is known to be described as a rotational mode figure b17. The second two modes come across $k=1$, the first one involves the rotation motion of the ring around radial axis. See figure 2b the Appendix A

Finally the second mode of $k=1$, is given by displacement of the ring radial direction, the motion is excited by the radial force applied on tread centerline. See figure 2b Appendix A

In summary, vibration behavior of the tire below 80 Hz is quite straightforward, the tire vibration has a semi rigid behavior. The Waves cross-section modes involve semi-rigid motion of the belt and have symmetric and anti-symmetric character.

7.3 Simulated results and validation

In order to validate the implemented model, simulated point and transfer mobility were compared to the corresponding measured quantities. The measurements data of the freely suspended tire are presented in section 7.1, while the measured data of the fixed rim tire are provided by Continental, due to the difficulties in realizing a clamped rim condition. Figure 18 the vibration orders and its corresponding frequency from the simulation result and the measurement's results (which has been provided by Continental) are compared, as can be seen each dot resemble the mode shape order versus its frequency. The blue dotted line resembles the simulation results, while the upper green line resemble the experimental results. From figure 18, it can be seen all modes from the buildup FE model occurs at lower frequencies compared to the measurements, which can indicate for a first glance that the tire model can be either softer or heavier than what supposed to be.

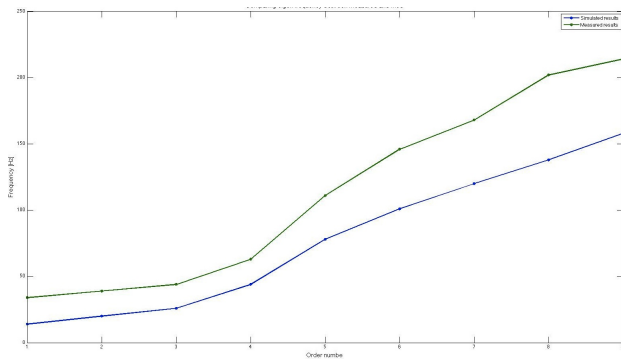


Figure 18: Comparison between measured and modeled vibration order, and its corresponding eigenfrequency. X-axis is vibration order in Hz Y-axis frequency in [Hz]

However, in the frequency response comparison, the resultant mobility form the simulation and measured point mobility the in house experiment (the results in section 7.1), provide with a closer look about the deviation in figure 18. An assessment of measured and modeled point mobility are displayed in Fig 19. The damping factor in the FE model η was assigned to a constant value of 0.5, and the maximum eigenfrequency which corresponds the eigen mode was 230 Hz mode. In the low-frequency range, spanning from 0 to some 50 Hz, the measured response can not be well reproduced. The reason is that in this frequency region, the measured tire is significantly affected by the finite rim mass and acts as a mass springmass system. In the simulation, however, by blocking the tire displacements at the beads, the rim mass is assumed infinite. Due to these differences, simulated results are not displayed over the first part of the low-frequency range. The modes located between 50 and 200Hz are seen to be fairly well predicted with respect to their natural frequencies except the

magnitude of mobility. However, this difference in magnitude was found about 6 dB which can indicate that half of energy is lost, that deviation is partly explained at the higher frequency, by the different level of local deformation in simulation and experiment, as a result of different ways of excitation. To be specific in the measurement, the load were applied on 16×16 mm aluminum plate, while in simulation, the excitation was modeled as an ideal point load. Figure 20 shows the point mobility comparison after adding 6 dB to the mobility, which shows a better matching in the amplitude.

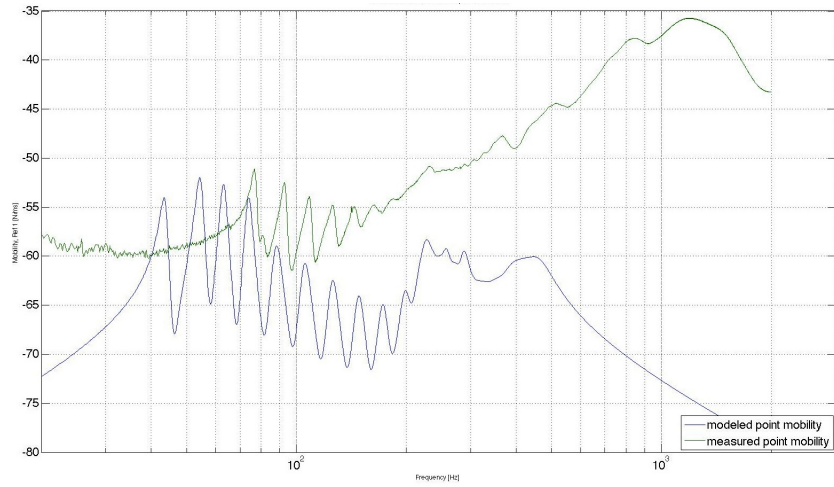


Figure 19: Comparison between the results of the measured point mobility and the real part of the radial point mobility from the FE model. X-axis is frequency in Hz Y-axis is mobility L_y in [dB] ref [1m/N.s]

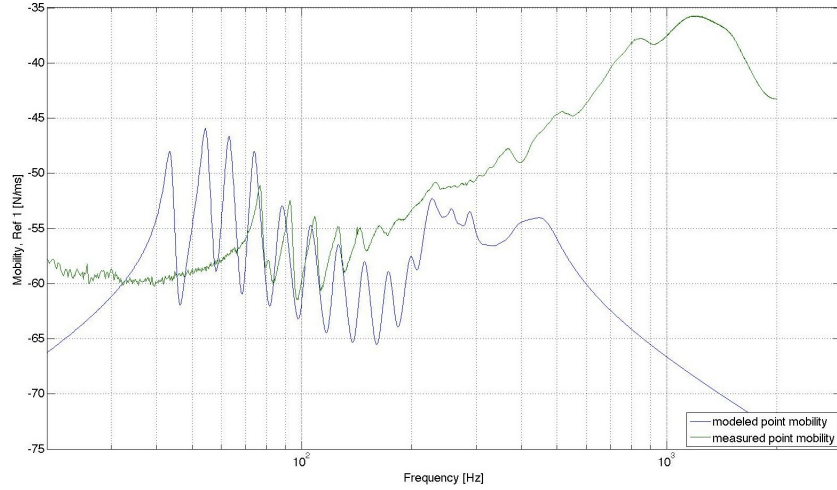


Figure 20: Comparison between the results of the measured point mobility and the real part of the radial point mobility from the FE model, after adding 6dB to the modeled mobility. X-axis is the frequency in Hz, Y-axis is mobility L_y in [dB] ref [1m/N.s]

In addition to the point mobility, Figure 21 depict the transfer point mobility at point separated by a distance of $(\pi/2 \times \text{Radius})$. However, the simulation result of transfer mobility function shows a better matching with measured values, compare to the results of simulated point mobility, which in turn emphasizes of the local deformation explanation about the modeled results in point mobility. Still by adding 6 dB to the displacement value of simulated transfer mobility, the amplitude of simulated values become a higher than the measured values. See figure22,

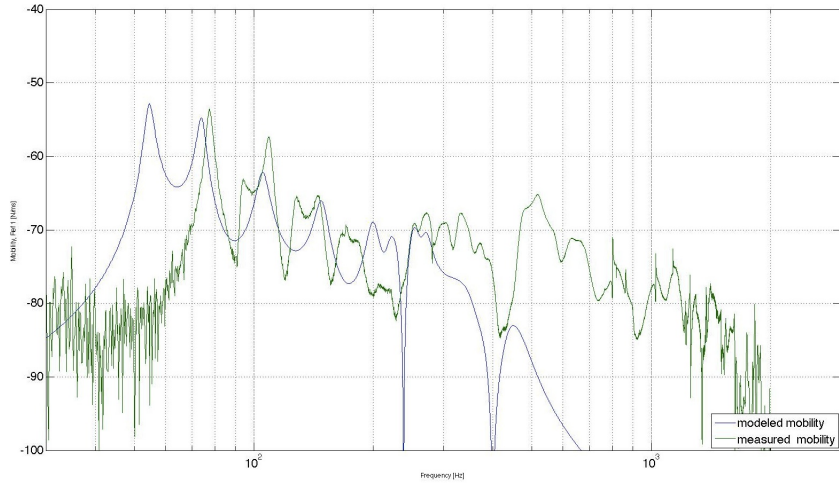


Figure 21: Comparison between the results of measured transfer mobility and the real part of the modeled transfer mobility. X-axis is the frequency in Hz Y-axis is mobility L_y in [dB] ref [1m/N.s]

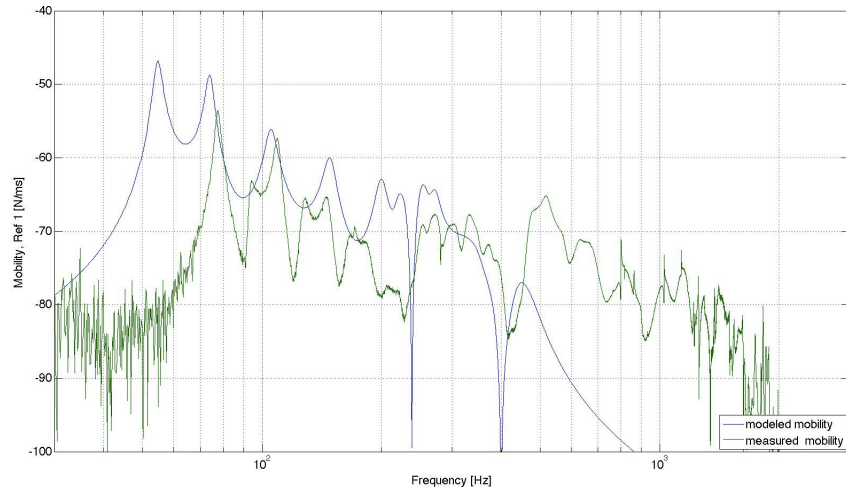


Figure 22: Comparison between the results of measured transfer mobility and the real part of the modeled transfer mobility, after adding 6dB to the modeled mobility. X-axis is frequency in Hz Y-axis is mobility L_y in [dB] ref [1m/N.s]

Likewise in section 7.1, the mobility function from the simulation is reported at different pressure levels as can be seen in figure 23. Same as with experimental results, the eigenfrequency in the model increases proportionally with pressure.

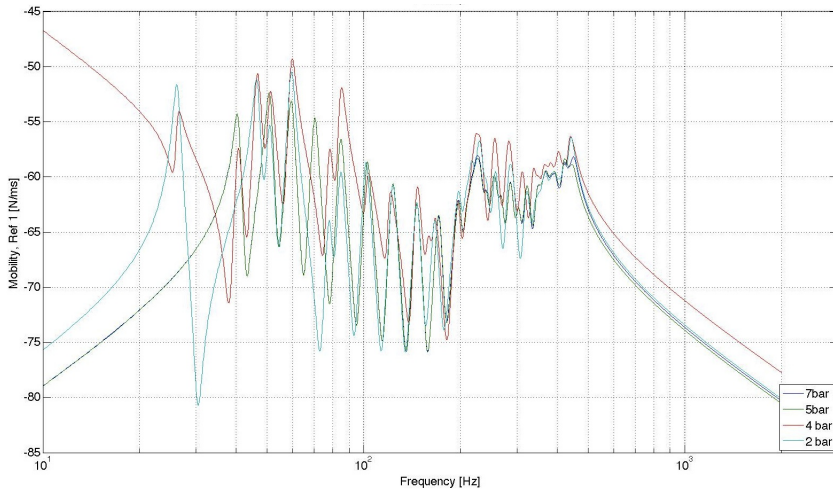


Figure 23: Modeled point mobility at different pressure levels.

However, the results which can be seen in figure 23 , does not match exactly with the experiment results in figure 12, a variance in the stiffness-pressure proportionality relation in the experiment and the simulation. This indicate that stiffness results from pre-tension study step was not calculated precisely, which in turn affect extraction of stiffness matrix in the free vibration study step. The pretension step is crucial in the computation precision of the final step in modeling vibration behavior of pre-stress structure. The reason for the inexact pre-stress calculation in the Finite Element Model possibly because of: First, the low mesh quality especially in hot spot regions (belts and ply) which can lead to high approximation tolerance in the stress calculations in the iteration process.

Second the linear elastic modeling for the rubber compound, which has been chosen as an approximation due to its simplicity in the analysis process.

However, the investigation of these two reasons hasn't been considered in this report, it's based on theoretical assumption and literature studies.

8 Conclusions

The measurement results can successfully be used for further simulations and validations where it can be seen from the coherence function, that a suitable correlation between measured force input function and output acceleration function from accelerometer. Although, the initial simulation results show some deviation from measurements (e.g. half of energy is missing), still the dynamic behavior of the model is taking the same pattern compared to measurement. The potential reasons for this division can be referred to the low mesh quality, which has effect on the accuracy in the first step of the simulation, this lead to an error in the stress computations especially in the hot spot areas like belts, and ply, which has even lower mesh quality. Numerical stability was a focal issue faced during this work, convergence to the right solution, was not easily achieved. The solver was converting from linear to nonlinear computations during the computation of the first simulation step(tire inflation). Even though, the simulation was assigned to linear elastic, which indicate that the compatibility criteria was not completely full filled. In other word, gaps between the elements are formulated during the meshing process.

Low mesh quality influence on the solving process, it led to a high number of iterations, which means a higher computation cost.

Therefore, future work advice:

Fixing the element of the model mesh and increase the number of the elements in the hot spot, in order to get a higher precision in the stress calculations which reflect more accuracy in stiffness matrix extraction.

Many obstructions were encountered during this work, but one of them, which has not been precisely confirmed, is to get the right mechanical properties of the compound materials. There were not a clear figures about the values of the stiffness and mass density of the tread and sidewall, this should be given more investigation, since it plays an important role in extracting the right stiffness matrix for the right calculation of a dynamic behavior of any structure .

9 References

- [1] = TA2 - Laboratory work on Statistical Energy Analysis, part 1. Chalmers university of technology. Gothenburg Sweden
- [2] = P. Sabiniarz - Modeling the vibration on a rolling tyre and their relation to exterior and interior noise . Division of applied acoustics, Vibroacoustic research group, Chalmers university of technology. Gothenburg Sweden 2011
- [3]= P. Sabiniarz, W. Kropp -A wave guide finite elemnet aided analysis of the wave field on a stationary tyre, not in contact with ground. Chalmers university of technology. Gothenburg Sweden
- [4] = Wolfgang Kropp - Script of Technical Acoustics 1. Chalmers university of technology. Gothenburg Sweden
- [5] = demeter g.fertic - dynamic and vibration of the structure. Wiley publications,ISBN 0-471-25777-X, 1973
- [6] = Chalmers - Numerical methods from Euler to FEM. Devision of Acoustics. Chalmers university of technology. Gothenburg Sweden
- [7] = P. Dinkova- Truck Tire Vibration Behavior. Measurements and modeling, Division of Applied Acoustics, Jan 2006
- [8] = C. Hoever - Derivations of the Finite Difference and Finite Element Methods as shown in the TA2 lectures, Division of Applied Acoustics, Jan 2012
- [9] = C. Hoever - Numerical methods for acoustical problems, Division of Applied Acoustics, 2012
- [10] = Cremer, Heckl, Petersson - Structure-Borne Sound, Springer-Verlag Berlin Heidelberg, 2005
- [11] = P. Thorsson - The wave approach for vibration calculations. Chalmers university of technology. Gothenburg Sweden,2004
- [12] = J.Halpin, Primer on composite materials analysis, Technomic Publishing company, Lancaster, Basel, 2nd edition,1992.
- [13] = PHYSICS OF CONTINUOUS MATTER, www.cns.gatech.edu , 2013
- [14] =P. Andersson, K. Larsson - "Validation of a High Frequency Three Dimensional Tire Model. *Acta Acustica united with Acustica* 91. pp.121-131,2005

[15]= Alan F.bower- Applied Mechanics of Soild- A.F. Bower (2012). Solid-Mechanics.org

[16]= Olaf Schenk and Klaus Gartner, PARDISO User Guide Version 4.1.2, Feb 12th 2011

[17]= Comsol Multiphysics 4.3b user manual. May 2013

[18]= C.Hover The influnce of modellin parameters on the simulation of car tyre rooling lose and rolling noise, Licenciate thesis. December 2012

[19]= A.Alipour and F.Zareian. STUDY RAYLEIGH DAMPING IN STRUCTURES; UNCERATINTIES AND TREATMENTS. May 2013

[20]= http://www.continental-specialtytires.com/www/industry_use_n/general/technical/tireconstruction_en.html. July 2013

[21]= <http://auto.howstuffworks.com/tire1.htm>. April 2013

Appendix A

Appendix A shows all extracted mode shapes from the FEM tire model are presented in Appendix A, some of these mode shapes are duplicated by a phase shift.

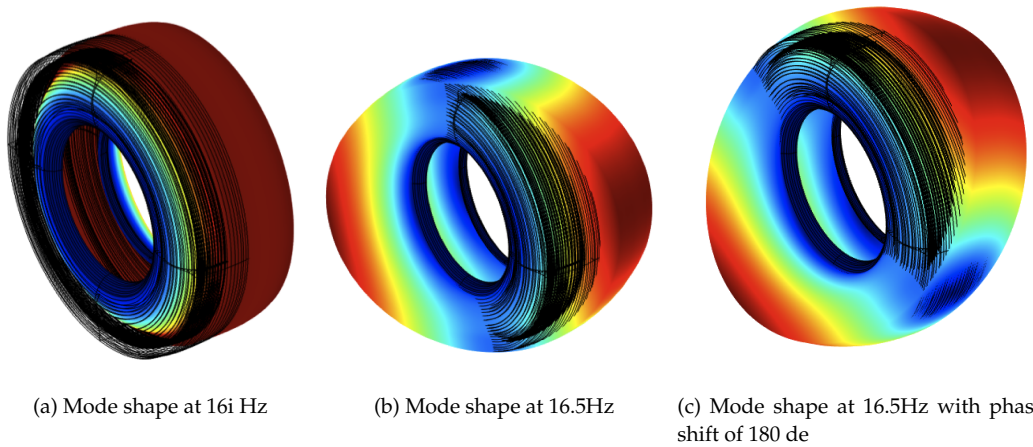


Figure 1: Semi rigid body motion modes

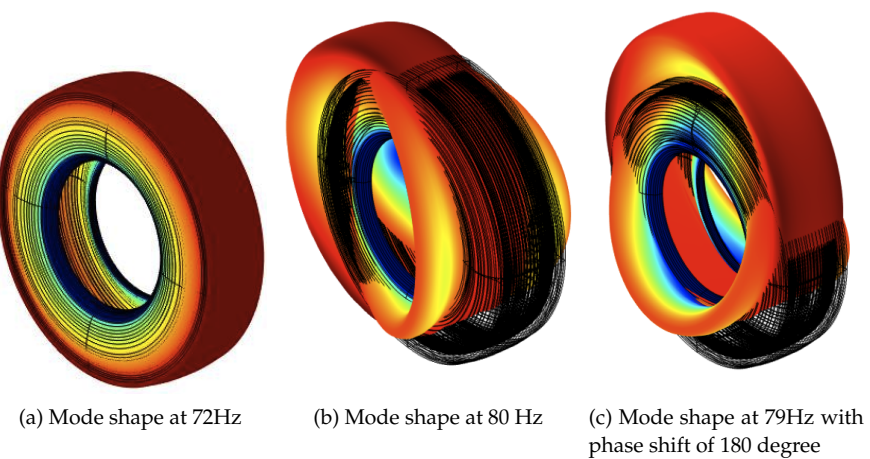


Figure 2: Semi rigid body motion modes

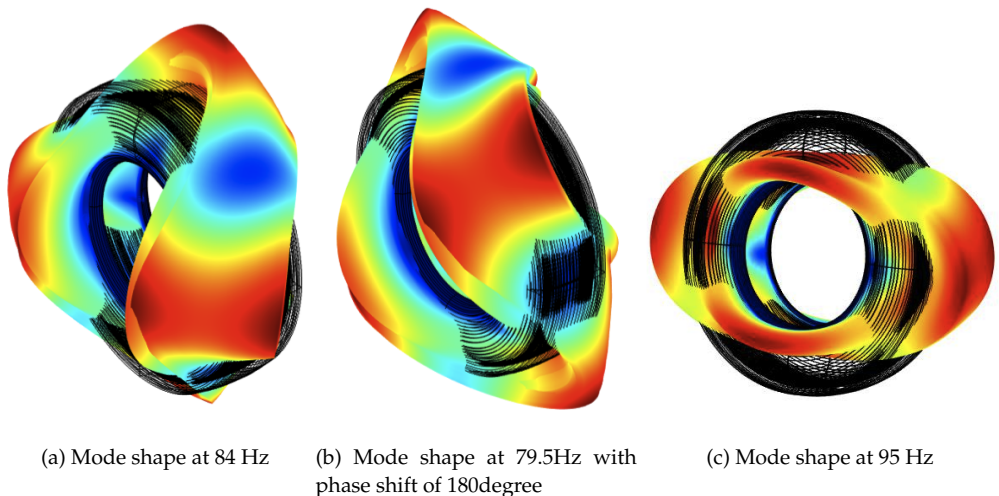


Figure 3: Free body motion modes

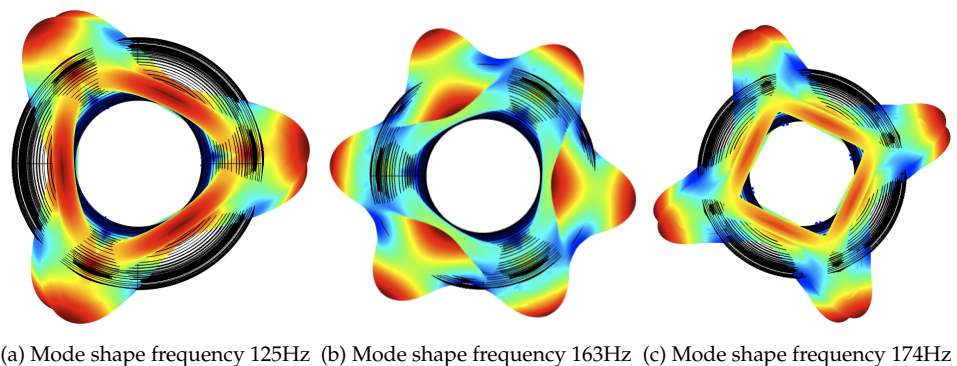
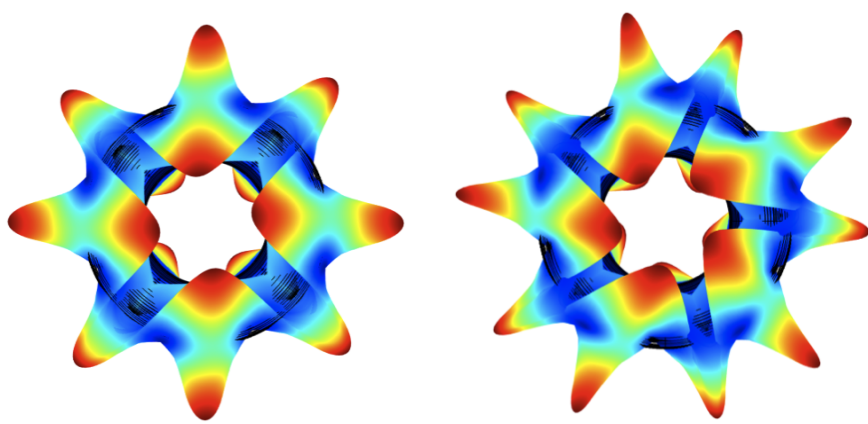


Figure 4: Free body motion modes



(a) Mode shape frequency 210Hz

(b) Mode shape frequency 230Hz

Figure 5: Free body motion modes

Appendix B-Matlab code

The details are tabulated in the softcopy attached with report